Steel Research International, doi: 10.1002/srin.201400318 (2015)

A three dimensional cellular automata model for dendrite growth in non-equilibrium solidification of binary alloy

Yan Zhao[a,*], Rongshan Qin[b] , Dengfu Chen[c], Xinming Wan[a] , Yang Li[a], Mingtu Ma[a]

[a] *Automotive lightweight Engineering Research Center, China Automotive Engineering Research Institute Co. Ltd, Chongqing 401122, P.R. China.*

[b] *Department of Engineering and Innovation, Open University, Walton Hall, Milton Keynes, MK7 6AA, United Kindom.*

[c] *Laboratory of Metallurgy and Materials, College of Materials Science and Engineering, Chongqing University, Chongqing 400030, P.R. China.*

Corresponding author. Tel.: +86 23 68652804.

E-mail *address*: zhaoyansuli1984@163.com (Yan Zhao).

Abstract

A three dimensional (3D) cellular automata (CA) model has been developed for simulation of dendrite growth during non-equilibrium solidification. The heat and mass transports are calculated using 3D finite element (FE) method. The migration of solid/liquid (SL) interface is associated with effective free energy difference incorporating solute trapping and relaxation effects. The non-equilibrium solute partition coefficient involving solute trapping and relaxation effects is used to calculate solute redistribution at SL interface. The interface curvature and anisotropy of surface energy are introduced to represent the characteristics of dendrite tip. The CA model has been applied to simulate the microstructure evolution of Fe-1.5 wt. % C alloy. The grain morphology, solute and temperature distributions, and velocity of dendrite tip are characterized during both isothermal and non-isothermal conditions. The velocity of dendrite tip and secondary dendrite arm spacing during directional solidification are validated and are in good agreements with previous experimental and mathematical results.

Keywords: Cellular automata; Finite element method; Dendrite growth; Non-equilibrium; Solidification microstructure

1. Introduction

Dendrite growth is one of the most important crystallization mechanisms in

casting and welding processes. The grain morphology, solute segregation and porous formation during dendrite growth in non-equilibrium solidification significantly affect the quality of final product. A number of mathematical models have been developed to predict the relationship between processing parameters and dendrite evolution since the 1950s [1-4]. Sharp interface model [5], level set model [6], phase field model [7, 8] and cellular automata (CA) model [9, 10] have been applied to the simulation of meso-scale dendrite growth. Quantitative simulation of dendrite growth in a macroscopic system with feasible computational cost is a challenge. Among those available mesoscopic methods, CA model possesses the simplest evolution mechanism, i.e. symbolic dynamics nature [11], and hence has the potential to simulate a larger system with minimal computing power. The problem of CA model is how to capture more features of dendrite in order to reveal the microstructure evolution, which is essential for macro-scale solidification practice.

The conventional CA models calculated the migration rate of solid/liquid (SL) interface according to Kurz-Giovanola-Trivedi (KGT) theory. This implies that the migration rate of SL interface is a function of initial undercooling. Gandin and Rappaz [12] developed a two dimensional (2D) CA model coupled with finite element (FE) method and simulated the grain growth in a non-isothermal system. FE method was used to calculate the heat transfer. The decentered-square growth algorithm was developed for the simulation of various crystal orientations. The 2D CA-FE model reproduced the grain structure and columnar-to-equiaxed transition (CET) with reasonable agreements with their experimental results. Zhu and Hong [13] developed a

three dimensional (3D) modified CA model and incorporated thermal, constitutional and curvature undercoolings. The SL interface velocity is related to initial bulk undercooling and interfacial kinetics contribution. In fact, KGT model is an analytical solution assuming dendrite tip grows at steady state. The effect of solute diffusion on interfacial kinetics is ignored, i.e. all points at SL interface follow the same function without regarding the location dependence of interfacial kinetics properties [14]. Nevertheless, KGT model only provides a qualitative description for dendrite growth. Wang *et al* [15] developed a diffusion-controlled CA model coupled with finite difference (FD) method and the migration rate of SL interface was determined by both equilibrium solute concentration and interfacial curvature. The decentered-square growth technology was also modified on the basis of Gandin's model. Dong and Lee [16] used a CA-FD model to simulate the CET during directional solidification. The nucleation and dendrite growth regarding both solute and temperature redistributions were studied. The earlier CA models based on local solute conservation at SL interface actually assume the SL interface is at steady state belonging to equilibrium solidification. These models are not suitable for the simulation of non-equilibrium solidification and rapid quenching. Zhao *et al* [17] developed a 3D CA-FE model in which the SL interface velocity was derived according to the phase transition driving force. However, this model is still insufficient to describe non-equilibrium solidification at the thermodynamics point of view.

In the present work, a 3D CA-FE model has been developed to simulate dendrite

growth during non-equilibrium solidification. The interface kinetics is determined by effective free energy difference incorporating solute trapping and relaxation effects in a binary alloy. The non-equilibrium solute partition coefficient with solute trapping as well as relaxation effects is considered. The interfacial anisotropy and curvature are taken into account. The model has been applied to simulate the dendrite growth of Fe-1.5 wt.% C alloy under both isothermal and non-isothermal conditions. The grain morphology, solute and temperature redistributions in non-equilibrium solidification are studied and discussed. The growth rate of dendrite tip and secondary dendrite arm spacing in non-isothermal solidification are validated against experimental and mathematical results.

2. Model description

2.1. Heat and mass transfers

The heat and mass transfers during solidification are calculated using 3D FE method. The governing equation for heat transfer is given by

$$\rho C_p \frac{\partial T}{\partial t} = \lambda \nabla^2 \mathrm{T} + \rho L \frac{\partial f_S}{\partial t}, \tag{1}$$

where ρ is the density, C_p is the specific heat, λ is the heat conductivity, L is the latent heat and f_S is the solid fraction. The heat flux on the domain boundary is calculated as

$$-\lambda \frac{\partial T}{\partial n} = h(T - T_f), \tag{2}$$

where h is the convective heat transfer coefficient, n is the normal vector to the boundary, and T_f is the environmental temperature. During non-equilibrium

solidification, the classical Fick's law is no longer valid due to the relaxation effect of solute diffusion, if the velocity of SL interface is comparable with or even larger than that of solute diffusion in bulk liquid. The governing equation for solute transport in this case is as follows[18]

$$\frac{\partial C}{\partial t}+\frac{D\partial^2 C}{V_D\partial t^2}=D\nabla^2 C, \tag{3}$$

where C is the solute concentration, D is the solute diffusivity, and V_D is the solute diffusion rate in bulk liquid. The boundary condition for Eq. 3 is related to both the velocity and acceleration of SL interface, which is calculated via[18]:

$$-D\frac{\partial C}{\partial n}=（V+\frac{D}{V_D{}^2}\frac{\partial V}{\partial t})(C-C_S{}^*)+\frac{DV}{V_D{}^2}(\frac{\partial C}{\partial t}-\frac{\partial C_S{}^*}{\partial t}), \tag{4}$$

where V is interface velocity, $C_S{}^*$ is solute concentration on the solid-side of SL interface, $C_S{}^*=\mathrm{k}C_L{}^*$, and $C_L{}^*$ represents solute concentration on the liquid-side of SL interface. The non-equilibrium solute partition coefficient k was proposed by Sobolev, which is represented as [19]

$$\begin{aligned} &k=\frac{(1-V^2/V_D{}^2)k_e+V/V_{DI}}{1-V^2/V_D{}^2+V/V_{DI}}, \qquad V<V_D, \\ &k=1, \qquad V\geq V_D \end{aligned} \tag{5}$$

where V_{DI} is the interfacial solute diffusive velocity. The values of k_e at different temperatures are obtained from the thermodynamics software Factsage.

2.2 The governing rule for the CA model during non-equilibrium solidification

The computational domain of CA model composes of discrete and homogenous cubic lattices. The state of a lattice during the simulation of solidification can be solid, liquid or interface (named solid lattice, liquid lattice and interface lattice hereafter).

Initially, all lattices are defined to be at liquid state. The governing rule for the evolution of lattice state is as follows: if a lattice at liquid state becomes a nucleation site or is captured by a growing solid lattice, it will turn into solid state and its six closest neighbors, if any of them are still at liquid state, will switch into interface lattice. The SL interface locates between solid lattices and interface lattices, and advances towards the liquid phase region. The migration rate of SL interface affects the solid fraction of interface lattice. When the solid fraction of an interface lattice reaches 1, it is considered that the lattice is captured by the growing solid phase. The iteration continues until solidification is complete. The transient temperature and solute concentration at all lattices are updated simultaneously by FE calculation.

The governing rule for the CA model is sensitive to the migration rate of SL interface. The latter at non-equilibrium solidification is associated with the free energy minimization in phase transition, which is described by Turnbull as [20]

$$V = V_0[1-\exp(-\frac{\Delta G}{RT})], \tag{6}$$

where V_0 is the upper limit of SL interface velocity, R is the gas constant and T is the temperature of SL interface. ΔG is the effective free energy difference incorporating solute trapping and relaxation effects. For binary alloys, ΔG is given as [21]

$$\begin{aligned} &\Delta G = (1-C_L^*)\Delta\mu_1 + C_L^*\Delta\mu_2 + (C_L^* - C_S^*)(1-k)RT(\frac{V}{V_D}), \quad V < V_D \\ &\Delta G = (1-C_L^*)\Delta\mu_1 + C_L^*\Delta\mu_2, \quad V \geq V_D \end{aligned}, \tag{7}$$

where $\Delta\mu_1$ and $\Delta\mu_2$ are the chemical potentials of solvent and solute at SL interface, respectively. The thickness of diffusive SL interface is much smaller than

the size of CA lattice, therefore, C_L^* is assumed to be approximately equal to the concentration of interface lattice here, and $C_S^* = kC_L^*$. $\Delta\mu_1$ and $\Delta\mu_2$ are obtainable via the following equations [22]

$$\begin{aligned} \Delta\mu_1 &= RTIn\frac{(1-C_S^*)(1-C_L^{eq})}{(1-C_L^*)(1-C_S^{eq})} \\ \Delta\mu_2 &= RTIn\frac{k}{k_e} \end{aligned}, \tag{8}$$

where C_L^{eq} and $C_S^{eq} = k_e C_L^{eq}$ are the equilibrium solute concentration on the liquid-side and the solid-side of SL interface, respectively. Taking into account the effect of the curvature and the anisotropy of SL interface, C_L^{eq} is obtained via [23]

$$C_L^{eq} = C_0 + \frac{T_C^{eq} - T_{C_0}^{eq}}{m_L} + \frac{\Gamma K\sigma(\hat{n})}{m_L}, \tag{9}$$

where T_C^{eq} and $T_{C_0}^{eq}$ are the temperatures at liquidus in the equilibrium phase diagram when the solute concentrations are C and C_0, respectively. m_L is the slope of equilibrium liquidus curve. The equilibrium phase diagram is obtained from Factsage. Γ is the Gibbs-Thomson coefficient. K is the curvature of the SL interface. $\sigma(\hat{n})$ is the anisotropic interface energy and is described for cubic crystal as follows [24]

$$\sigma(\hat{n}) = k_0 + k_1\left(\hat{n}_x^2\hat{n}_y^2 + \hat{n}_y^2\hat{n}_z^2 + \hat{n}_z^2\hat{n}_x^2\right) + k_2\hat{n}_x^2\hat{n}_y^2\hat{n}_z^2 + k_3\left(\hat{n}_x^2\hat{n}_y^2\hat{n}_z^2\right)^2, \tag{10}$$

where $\hat{n}$ represents the local orientation of SL interface, $\hat{n}_x$, $\hat{n}_y$ and $\hat{n}_z$ are its Cartesian components. k_0, k_1, k_2 and k_3 are anisotropy coefficients whose values are available in Ref. [24]. The curvature of SL interface K is calculated by [25]

$$K = \frac{1}{\Delta s}\left[1 - \frac{2}{N+1}\left(f_S + \sum_{n=1}^{N} f_S^n\right)\right], \tag{11}$$

where Δs is the mesh size and N is the number of the neighbors.

The solid fraction f_s of cubic interface lattice at each time step is obtained via:

$$f_s = \frac{\Delta s^2 \Delta t (v_x + v_y + v_z) - \Delta s \Delta t^2 (v_x v_y + v_y v_z + v_x v_z) + \Delta s^3 \Delta t^3}{\Delta s^3}, \quad (12)$$

where v_i is the component of interface velocity along with i-direction. Δt is the time step.

3. Results and discussion

The dendrite growth during isothermal and non-isothermal solidifications is simulated using our in-house software compiled by Visual C++ 2010, which couples temperature and mass transports with the CA model. The temperature and mass fields are solved using FE method.

3.1. Isothermal dendrite growth

The model has been applied to simulate the growth of a single dendrite at different degrees of undercooling. The computational domain includes 40×40×40 lattices. The lattice size is usually determined by both the migration of SL interface and the accuracy of FE model. If the lattice size is too small, more than one liquid lattice might be captured by SL interface at one time step, even if some of them do not have solid neighbors, this is against the evolution rule in this model, i.e. the moving distance of SL interface at one time step should be much less than the lattice size. If the lattice size is too large, the numerical accuracy will be poor, which is related to mass transfer coefficient. In order to avoid the problems mentioned above, the lattice size is set as 3 μm after some trials prior to the simulation. Moreover, The lattice size always has inevitable effect on dendrite morphology owing to the numerical accuracy

of FE model and is difficult to completely eliminate. More and finer secondary dendrites are generated when lattice size is larger [17].The simulation is performed on Fe-1.5 wt.% C alloy and the physical parameters of this alloy used in the model is listed in Table 1. A solid seed is planted at the center of the domain. The isothermal assumption is fulfilled by assigning constant temperature lower than liquidus to all lattices at the beginning of solidification, and then dendrite growth is driven by given undercooling. Fig.1 represents the dendrite morphology at t = 0.01 s since the beginning of growth at various degrees of undercooling. It can be seen that undercooling significantly affects the dendrite morphology. The dendrite grows faster in the presence of a larger undercooling implying a larger phase transition driving force. It means that, compared to compositional and curvature undercoolings, thermal undercooling is still the dominant factor to determine the velocity of dendrite tip. There are more secondary arms formed in the liquid with a higher undercooling. This is due to the more instable interface caused by a lower solute diffusivity and a larger interface velocity at larger undercoolings. The results are consistent with Mullins and Sekerka's interface stability theory [26, 27]. Fig.2 shows the carbon distribution during dendrite growth at various undercoolings when t = 0.01s. The diffusive layers of concentration in front of SL interface are shown as well. The concentration gradient rises with the increasing undercooling. The highest concentration area locates among dendrite arms due to the expelling of carbon from solid phase. The pileup of concentration in front of SL interface makes the coarsening process of dendrite arm weaker at larger undercoolings. Fig.3 shows the growth rate of dendrite tip as a

function of solid fraction at various undercoolings when t = 0.01s. The dendrite tip starts to grow at a high speed and then reduces rapidly to a stable value. It is worth to note that, the velocity of dendrite tip with a larger undercooling experiences a faster decline as seen in Fig.3, this is mainly affected by compositional undercooling decreasing more rapidly in the case of a poorer solute diffusivity at SL interface, when thermal undercooling is larger. The average growth rate of dendrite tip at various undercoolings when t= 0.01s are illustrated in Fig.4. It can be seen that the growth velocity increases rapidly from about 0.00016 m/s at 10 K to 0.0218 m/s at 100K.

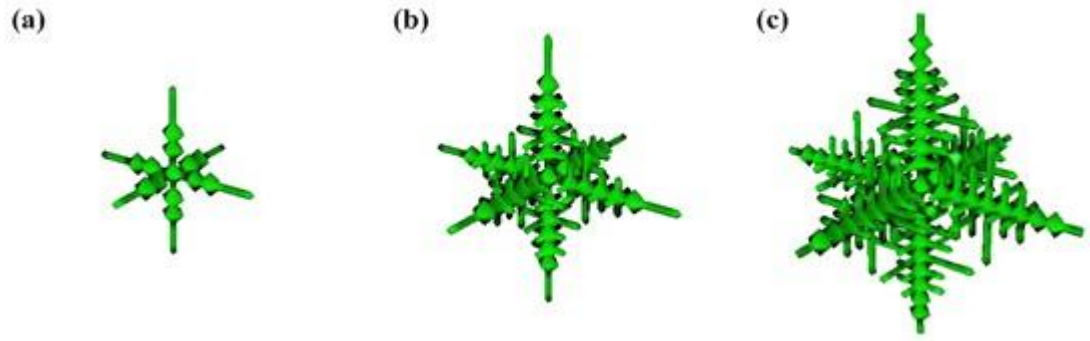

Fig.1. The morphology of the equiaxed dendrite at t = 0.01s growing at an undercooling of (a) $\Delta T = 50K$; (b) $\Delta T = 60K$; and (c) $\Delta T = 70K$.

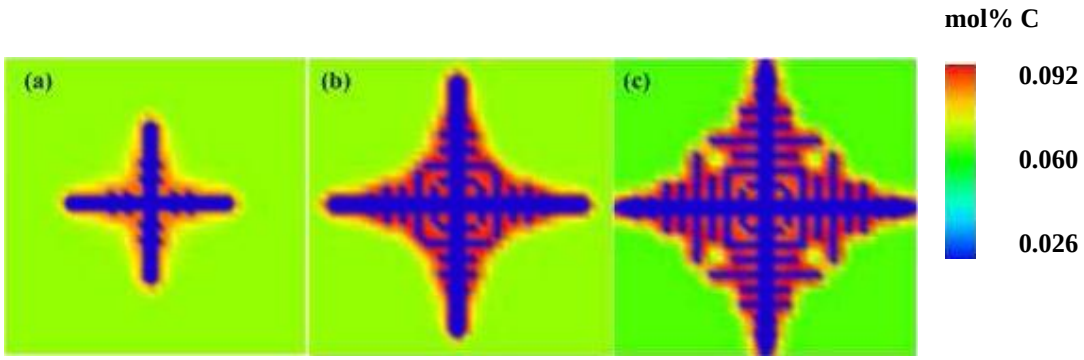

Fig.2. The carbon concentration profile of the equiaxed dendrite at t = 0.01s growing

from the liquid at an undercooling of (a) $\Delta T = 50K$; (b) $\Delta T = 60K$; and (c) $\Delta T = 70K$.

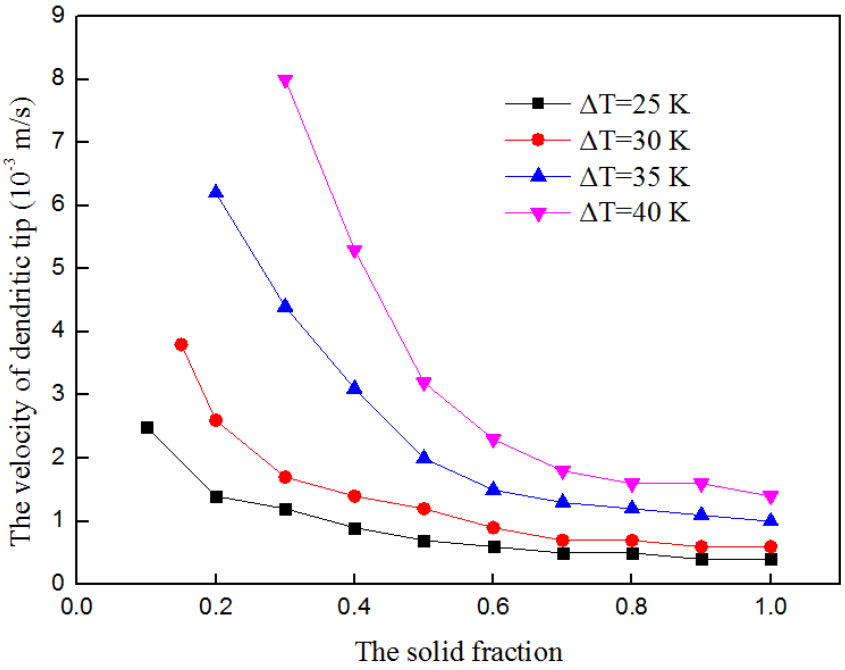

Fig.3. The velocity of the dendrite tip at t=0.01s as a function of the solid fraction at various undercoolings.

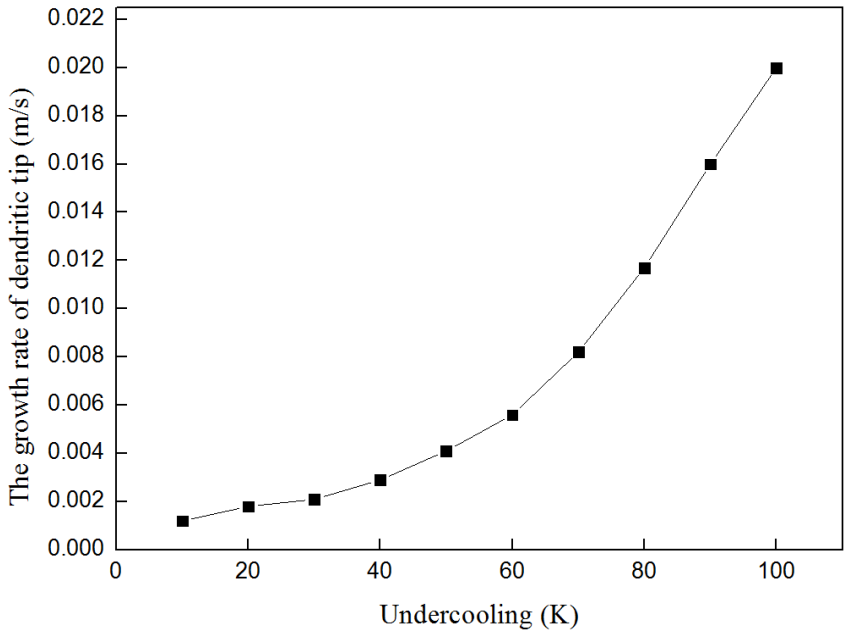

Fig.4. The average velocity of the dendrite tip at t = 0.01s at various undercoolings.

3.2. Non-isothermal dendrite growth

The simulation of non-isothermal dendrite growth is performed in a domain consisting of 15×45×40 lattices with the lattice size of 3 μm. The heat is transferred away from the domain via the bottom boundary with different transfer coefficients. The initial temperature of the domain is set to the melting temperature of 1420 ℃. Three solid nuclei are planted on the bottom boundary to simulate the directional dendrite growth during non-isothermal solidification. Fig.5 shows the numerical results at t = 0.036 s with various convective heat transfer coefficients. It can be seen that dendrites grow fastest along the vertical direction. The growth rate of dendrite tip is larger and more secondary arms are generated with larger convective heat transfer coefficients. It also indicates that SL interface becomes more instable with larger cooling rates. The carbon distribution during dendrite growth with various heat flow intensities at t = 0.036 s is illustrated in Fig.6. More solute is piled up between primary and secondary dendrite arms due to the interdendritic growth. The accumulation of the solute around dendrites reduces constitutional undercooling and hence restricts the growth of secondary arms. Fig.7 illustrates the temperature distribution profile during non-isothermal dendrite growth at t = 0.036 s. It can be seen in Fig. 7(b) and Fig. 7(c) that the temperature at primary dendrite tips is always the highest. This is mainly due to the release of largest amount of latent heat at the fastest growing dendrite tips during liquid-solid phase transition.

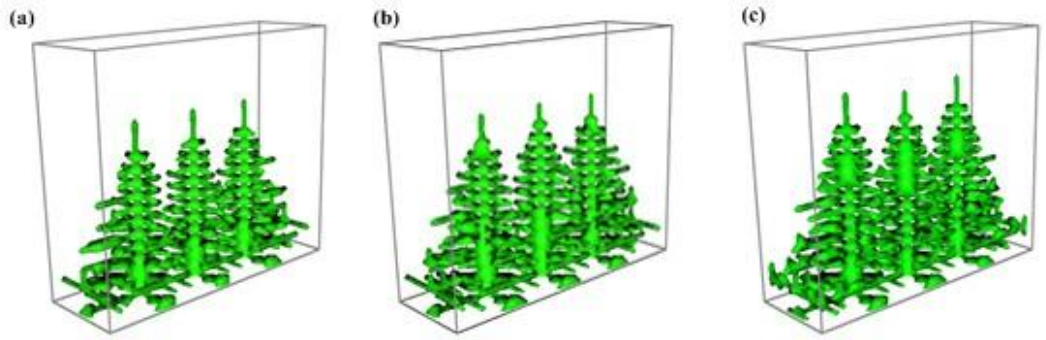

Fig.5. The dendrite morphology at t= 0.036 s growing with the convective heat transfer coefficient of (a) $h=1000Wm^{-2}K^{-1}$; (b) $h=1100Wm^{-2}K^{-1}$; and (c) $h=1200Wm^{-2}K^{-1}$.

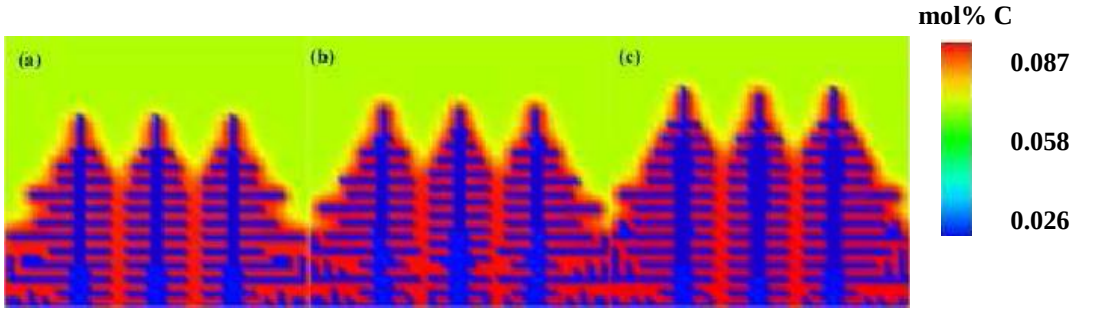

Fig.6. The carbon concentration profile at t = 0.036 s with the convective heat transfer coefficient of (a) $h=1000Wm^{-2}K^{-1}$; (b) $h=1100Wm^{-2}K^{-1}$; and (c) $h=1200Wm^{-2}K^{-1}$.

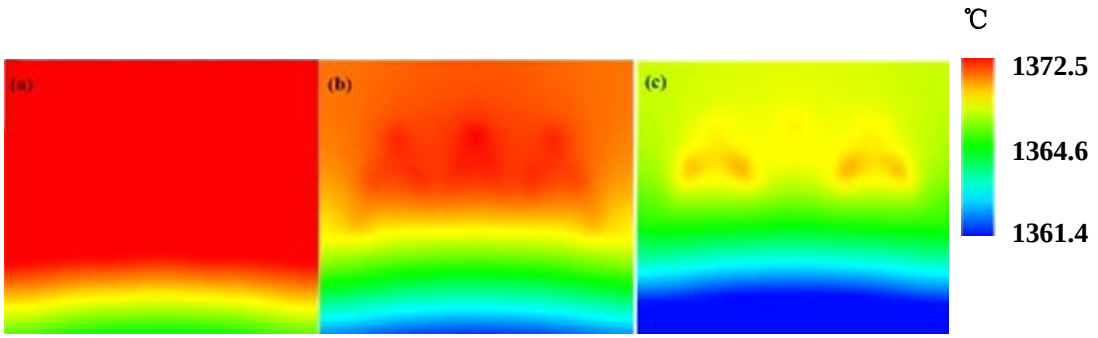

Fig.7. The temperature distribution at t = 0.036 s with the convective heat transfer

coefficient of (a) $h = 1000 Wm^{-2}K^{-1}$; (b) $h = 1100 Wm^{-2}K^{-1}$; and (c) $h = 1200 Wm^{-2}K^{-1}$.

3.3. Model Validation

To validate the developed CA model, the relationship between temperature gradient (G), growth velocity of dendrite tip (V) and secondary arm spacing obtained by the numerical calculations are compared with previous experimental results. The simulation is carried out in a logistical frame containing 10×10×20 lattices with the lattice size of 3 μm with various temperature gradients. The temperature gradient is generated by using different heat transfer coefficients on the bottom boundary of the domain. Suutala [28] reported the relationship between G and V in welding of low carbon steel as $\log G = 2 + \log V$ (G in K/mm and V in mm/s). Miettinen [29] measured G, V and primary dendrite arm spacing in directional solidification of Fe-1.5 wt.% C steel, in which the velocities of primary dendrite tip at temperature gradients of 278 K/mm, 495 K/mm and 635 K/mm were given. Owing to the different cooling conditions, fitting curve on the basis of experimental results in Ref. [29] is employed to validate the developed CA model. Fig. 8 presents the comparison between numerical results using the CA model and reported experimental results in Ref. [28, 29]. The results from the CA model have good agreements with Miettinen's experimental results but are slightly higher than that from Suutala's conclusion. This is mainly because the carbon content in Ref. [28] is different with that in the CA model, however, the overall trends of data are in good agreements. Jacobi *et al* [30] measured the secondary arm spacing of Fe-1.48 wt. % C steel in directional

solidification and obtained an expression as follows

$$\lambda = 0.00716 \times \theta_f^{0.50} (\mu m), \tag{13}$$

where λ is the secondary dendrite arm spacing, and θ_f is the local solidification time. EL-Bealy *et al* [31] proposed a mathematical approximation to predict the secondary arm spacing of Fe-1.5 wt. % C steel, and the equation is expressed as

$$\lambda = 7.42764 \times (\theta_f)^{0.52} (\mu m), \tag{14}$$

Fig.9 illustrates the secondary arm spacing distribution at various local solidification times calculated by the present CA model and by Ref. [30, 31]. The numerical results are slightly higher when local solidification time is less than 1 s, but are in good agreements thereafter.

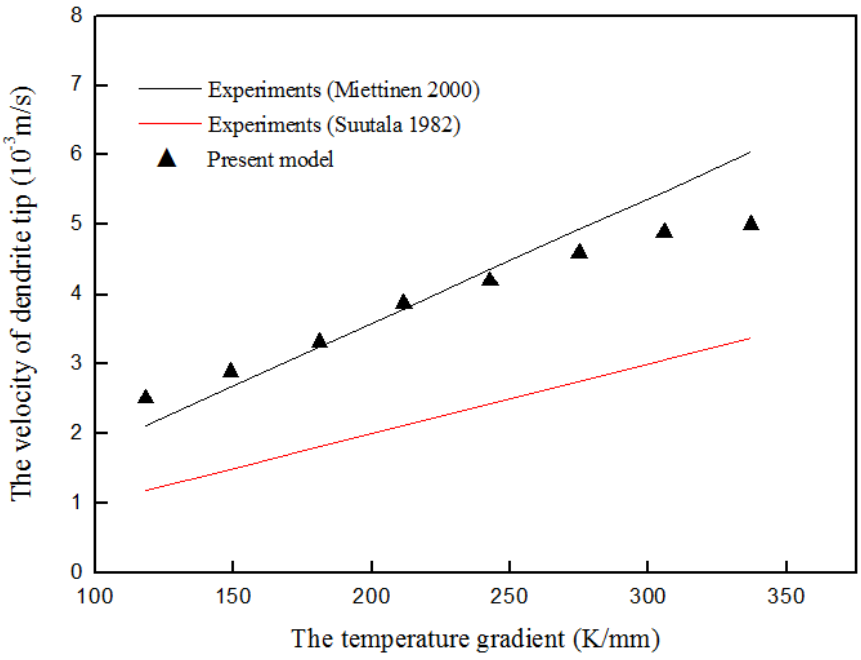

Fig.8 The velocity of the dendrite tip vs. the temperature gradient in directional solidification.

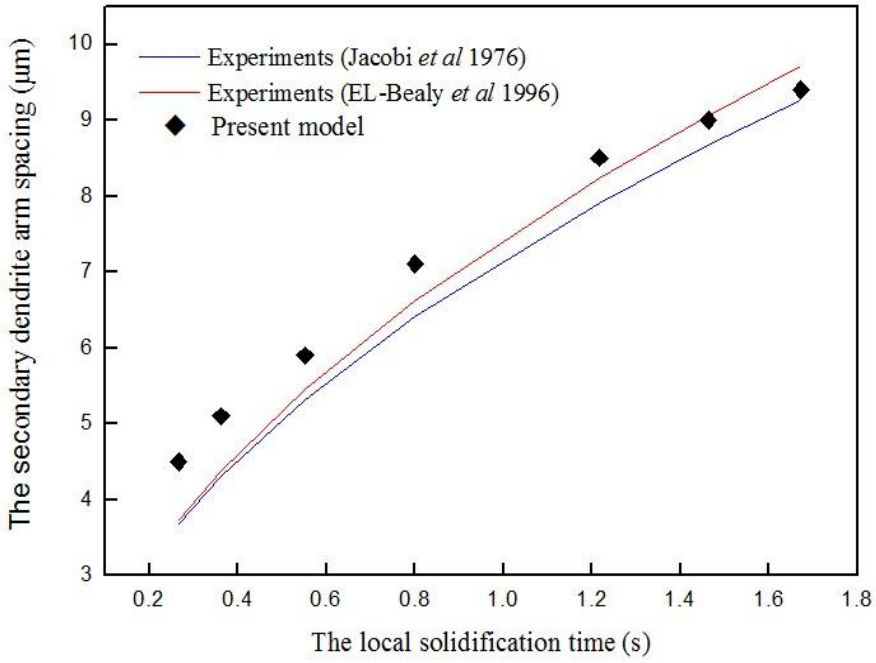

Fig.9 The dendrite secondary arm spacing vs. the local solidification time in directional solidification.

4. Conclusion

A 3D CA model for dendrite growth during non-equilibrium solidification of binary alloys has been developed. The heat and mass transfers are calculated using FE method. The migration of SL interface is calculated according to the driving effective free energy. The non-equilibrium solute partition coefficient with solute trapping is treated as a function of both SL interface migration rate and the equilibrium solute partition coefficient. The latter is obtained from the thermodynamics database Factsage. The effect of interfacial curvature and anisotropy of the surface energy are considered. The model has been applied to simulate isothermal and non-isothermal dendrite growth in Fe-1.5wt.%C alloy. In isothermal solidification, dendrite tip grows faster and more secondary arms are produced at a larger undercooling. The thermal

undercooling is the governing factor of dendrite tip velocity. The solute segregation is more severe in system at a larger undercooling. This is attributed to the lower solute diffusivity and the release of larger amount of solute at moving SL interface with a higher speed. The SL interface velocity starts at a high value but gradually decreases to a smaller but steady value as solid fraction increases in the isothermal domain, and the variation patterns of SL interface migration rate are mainly affected by compositional undercooling. The average velocity of dendrite tip rapidly increases along with the increasing undercooling, up to 0.0218 m/s at $\Delta T = 100K$. In non-isothermal solidification, the dendrite tip velocity is proportional to temperature gradient, and the preferred growth direction is opposite to the maximum heat flux direction. The carbon concentration is highest among secondary dendrite arms. The highest temperature in the domain appears at primary dendrite tips due to this being the local fastest release of latent heat during solidification. The developed CA model has been validated against earlier experimental and mathematical results on dendrite tip velocity and secondary arm spacing, respectively. The CA model shows good agreements with these existing results. The present model can be used to simulate the microstructure evolution under various cooling parameters in practical solidification.

Acknowledgement

Rongshan Qin is grateful to the support of TATA steel and the Royal Academy of Engineering at the UK. This work is financially supported by the Natural Science Foundation of China (NSFC, No.: 51374260), Chongqing Fundamental and Front

Research Plan- Outstanding Youth Project (No.: cstc2013jcyjjq60001) and Chinese Automotive Light-weight technology Research Institute Co. Ltd (No.: 20130205).

References

[1] J. Lipton, M.E. Glicksman, W. Kurz, *Mater. Sci. Eng.* **1984**, *55*, 57

[2] W. Kurz, D.J. Fisher, *Acta Metall.* **1981**, *29*, 11

[3] J. Lipton, W. Kurz, R. Trivedi, *Acta Metall.* **1987**, *35*, 957

[4] L. Beltran-Sanchez, D.M. Stefanescu, *Metall. Mater. Trans. A.* **2004**, *35*, 2471

[5] J.S. Langer, *Rev. Mod. Phys.* **1980**, *52*, 1

[6] Y.T. Kim, N. Goldenfeld, J. Dantzig, *Phys. Rev. E* .**2000**, *62*, 2471-2474.

[7] M.G. Mecozzi, J. Sietsma, S. van der Zwaag, Comp. *Mater. Sci.* **2005**, *34*, 290

[8] R.S. Qin, E.R. Wallach, *Acta Mater.* **2003**, *51*, 6199

[9] B. Su, Z. Han, B. Liu, *ISIJ Int*. **2013**, *53*, 527.

[10] B. Li, Q. Wang, F. Wang, M. Chen, *JOM*. **2014**, *66*, 1153

[11] W. Wolfram, *Rev. Mod. Phys.* **1983**, *55*, 601

[12] Ch.-A. Gandin, M. Rappaz, *Acta Mater.* **1994**, *42*, 2233

[13] M.F. Zhu, C.P. Hong, *ISIJ Int.* **2002**, *42*, 520

[14] L. Beltran-Sanchez, D.M. Stefanescu, *Metall. Mater. Trans. A.* **2003**, *34*, 367

[15] W. Wang, P.D. Lee, M. Mclean, *Acta Mater*. **2003**, *51*, 2971

[16] H.B. Dong, P.D. Lee, *Acta Mater.* **2005**, *53*, 659

[17] Y. Zhao, R.S. Qin, D.F. Chen, *J. Cryst. Growth*. **2013**, *377*, 72

[18] S.L. Sobolev, *Phys Lett A*. **1995**, *199*, 383-386.

[19] S.L. Sobolev, *Phys Rev E*. **1997**, *55*, 6845.

[20] D. Turnbull, *J. Phys. Chem.* **1962**, *66*, 609

[21] S. Li, J. Zhang, P. Wu, *J. Cryst. Growth*. **2010**, *312*, 982

[22] H. Wang, F. Liu, Z Chen, G. Yang, Y. Zhou, *Acta Mater*. **2007**, *55*, 497

[23] M.F. Zhu, D.M. Stefanescu, *Acta Mater*. **2007**, *55*, 1741

[24] R.S. Qin, H.K.D.H. Bhadeshia, *Acta Mater*. **2009**, *57*, 2210

[25] L. Nastac, *Acta Mater*. **1999**, *47*, 4253

[26] W.W. Mullins, R.F. Sekerka, *J. Appl. Phys*. **1963**, *34*, 323

[27] W.W. Mullins, R.F. Sekerka, *J. Appl. Phys.* **1964**, *35*, 444

[28] N. Suutala, *Metall. Trans. A.* **1983**, *14*, 191

[29] J. Miettinen, *Metall. Trans. B.* **2000**, *31*, 365

[30] H. Jacobi, K. Schwerdtfeger, *Metall. Trans. A.* **1976**, *7*, 811

[31] M. EL-Bealy, B.G. Thomas, *Metall. Trans. B.* **1996**, *27*, 689